

Conserved Signal Transduction Mechanisms and Dark Recovery Kinetic Tuning in the *Pseudomonadaceae* Short Light, Oxygen, Voltage (LOV) Protein Family

Vladimir Arinkin 1,† , Joachim Granzin 1 , Karl-Erich Jaeger 2,3 , Dieter Willbold 1,4 , Ulrich Krauss 2,3,5 and Renu Batra-Safferling 1,*

- 1 Institut für Biologische Informationsprozesse (IBI): Strukturbiochemie (IBI-7), Forschungszentrum Jülich, 52425 Jülich, Germany
- 2 Institut für Molekulare Enzymtechnologie, Heinrich-Heine-Universität Düsseldorf, Forschungszentrum Jülich GmbH, 52425 Jülich, Germany
- 3 Institut für Bio- und Geowissenschaften (IBG): Biotechnologie (IBG-1), Forschungszentrum Jülich GmbH, 52425 Jülich, Germany
- 4 Institut für Physikalische Biologie, Heinrich-Heine-Universität Düsseldorf, 40225 Düsseldorf, Germany
- 5 Department of Biochemistry, University of Bayreuth, 95447 Bayreuth, Germany

Correspondence to Renu Batra-Safferling: r.batra-safferling@fz-juelich.de (R. Batra-Safferling) https://doi.org/10.1016/j.jmb.2024.168458

Edited by Volha Chukhutsina

Abstract

Light-Oxygen-Voltage (LOV) flavoproteins transduce a light signal into variable signaling outputs via a structural rearrangement in the sensory core domain, which is then relayed to fused effector domains via α-helical linker elements. Short LOV proteins from *Pseudomonadaceae* consist of a LOV sensory core and N- and C-terminal α-helices of variable length, providing a simple model system to study the molecular mechanism of allosteric activation. Here we report the crystal structures of two LOV proteins from Pseudomonas fluorescens - SBW25-LOV in the fully light-adapted state and Pf5-LOV in the dark-state. In a comparative analysis of the Pseudomonadaceae short LOVs, the structures demonstrate lightinduced rotation of the core domains and splaying of the proximal $A'\alpha$ and $J\alpha$ helices in the N and Ctermini, highlighting evidence for a conserved signal transduction mechanism. Another distinguishing feature of the Pseudomonadaceae short LOV protein family is their highly variable dark recovery, ranging from seconds to days. Understanding this variability is crucial for tuning the signaling behavior of LOVbased optogenetic tools. At 37 °C, SBW25-LOV and Pf5-LOV exhibit adduct state lifetimes of 1470 min and 3.6 min, respectively. To investigate this remarkable difference in dark recovery rates, we targeted three residues lining the solvent channel entrance to the chromophore pocket where we introduced mutations by exchanging the non-conserved amino acids from SBW25-LOV into Pf5-LOV and vice versa. Dark recovery kinetics of the resulting mutants, as well as MD simulations and solvent cavity calculations on the crystal structures suggest a correlation between solvent accessibility and adduct lifetime. © 2024 The Author(s). Published by Elsevier Ltd. This is an open access article under the CC BY license (http://creativecommons.org/licenses/by/4.0/).

Introduction

Light, oxygen, voltage (LOV) domain containing flavoproteins are ubiquitous photoreceptors, whose signal-transducing LOV domains belong to the period circadian protein (Per)-aryl hydrocarbon receptor nuclear translocator (Arnt)-single minded protein (Sim) (PAS) superfamily. Functionally versatile, multidomain sensory LOV photoreceptors consist of at least one structurally conserved sensor

LOV domain, which is in most cases linked to diverse effector domain(s). The sensor domain binds a small molecule ligand, such as flavin mononucleotide (FMN) or flavin adenine dinucleotide (FAD), responsible for signal perception upon absorption of blue light. Light absorption by the flavin chromophore triggers a series of photophysical and photochemical steps that eventually lead to the formation of a covalent bond between the flavin chromophore and a conserved cysteine residue in the LOV domain $^{3-5}$ accompanied by a conformational change of a conserved glutamine residue, although both residues have been deemed dispensable for LOV signal transduction. 6,7 FMN-Cys adduct formation in turn results in global structural rearrangements in the LOV domain. This signaling-state, as the longest lived intermediate of the LOV photocycle represents in most cases the biologically active state, where the structural changes in the LOV domain are transmitted to fused effector domains^{8,9} or downstream signaling partner proteins. 10,111 As illumination ceases, the FMN-Cys adduct is thermally broken and the initial dark state is recovered with a characteristic time constant often reported as the adduct-state lifetime or dark recovery.

Recent studies have shown that the dark recovery process, involving both the thermal rupture of the FMN-Cys and reversal of the global structural changes associated with signaling state formation, is a complex multi-step process 12-14 that impacts biological function by providing a handle to impart different light sensitivities to the photoreceptor. 15-17 Even though, many mechanistically-driven mutational studies of the dark recovery process have been conducted, 18-31 the dark recovery is still not completely understood. Various mechanisms that modify the dark recovery have been presented: identifying the hydrogen-bond or salt-bridge network surrounding the chromophore, 18-2 interactions affecting the conformation of the adduct forming cysteine, as well as the conformational freedom of the flavin, 5,23-26 and lastly, factors that influence the deprotonation of the flavin N5 atom, e.g., pH, buffer, imidazole, hydration or water/solvent access to the flavin^{3,27–31} as instrumental for dark recovery tuning.

While the initial photochemical steps leading to the formation of the covalent protein-flavin adduct are likely conserved across the LOV family of photoreceptors, the intramolecular signal relay mechanisms in the LOV domain and associated effector domains might be distinct, even though they display conserved features such as short N-and C-terminal extensions that transduce the signal. This may account for the modularity of the LOV photoreceptor family, in which a structurally conserved LOV domain controls the activity of a variety of different effector domains.

As light-dependent signaling receptors, LOV domains regulate a myriad of light responses, e.g.

phototropism, chloroplast movement, and stomatal opening in plants^{32,33}; photomorphogenesis in stramenopile algae, 34 circadian rhythms and transcription regulation in fungi³⁵; stress responses, virulence and cell adhesion in bacteria. 9,30,36 In most cases, LOV photoreceptors are multidomain proteins that contain at most two, mostly Nterminal LOV domains that have short N- and Cterminal extensions outside the canonical LOV domain (termed A' α and J α -helix), which are involved in intramolecular signaling and effector domain activation.^{37,38} In addition, inverted architectures exist, such as algal aureochromes, in which the LOV domain is located at the Cterminus of the effector domain,34 and so-called short LOV proteins have been identified in bacteria. fungi, protists, and land plants that consist of only a single LOV domain and lack a fused effector domain but instead contain only N- and C-terminal $A'\alpha$ and $J\alpha$ helices.^{23,39-46} So far, physiological functions could only be assigned to a few short LOV proteins. For example, VVD, a short LOV protein, which possess a N-terminal A'α extension, but lacks the C-terminal $J\alpha$ -helix, ⁴⁷ modulates gating of the circadian clock via interaction with the White-Collar Complex (WCC), the central transcription factor of the circadian clock in fungi such as Neurospora crassa.47 DsLOV, another short LOV protein from a marine phototrophic bacterium Dinoroseobacter shibae, which, like VVD, only contains a N-terminal A'α-helix, mediates lightdependent pigmentation, 44 while the RsLOV protein purple photosynthetic bacterium from the Rhodobacter sphaeroides, which contains a short A'α-helix N-terminal and longer helix – turn – helix motif composed of helices Ja and Ka,48 was suggested to act as a repressor of photosynthesis gene expression and was linked to photooxidative damage responses, carbohydrate metabolism, and chemotaxis. 49,50 A recent report on the saprotrophic soil bacterium Pseudomonas putida KT2440 suggests that the two PpSB-LOV proteins and three PpIRs (Pseudomonas putida light-inducible transcriptional regulators) cooperatively regulate the light-inducible expression of a number of genes encoding DNA-photolyases, the furan-containing fatty acid synthase FolE, a GTP cyclohydrolase I, a cryptochrome-like protein, and various genes of unknown function.⁵¹ A similar role has recently been attributed to the short LOV protein PmSB-LOV of Pseudomonas mendocina.11 Thus, there is growing evidence for distinct lightdependent biological functions of a variety of Pseudomonadaceae short LOV proteins.

Up to now, five short LOV proteins from different *Pseudomonas* species were spectroscopically characterized, suggesting an evolutionary conservation of fast- and slow-reverting short LOV proteins in *Pseudomonadaceae*.⁴¹ Apparently, evolutionary pressure exists to select for fast and slow reverting LOV proteins linked to different physiolog-

ical functions in *Pseudomonadaceae*. This feature. at the same time, renders the *Pseudomonadaceae* short LOV protein family a paradigm for studying the LOV domain dark recovery process. All five sequences show the classical features of the Pseudomonadaceae short LOV protein family, i.e., Y(Q/ R)DCRFLQG motif in the LOV core domain, a conserved N-cap, and the C-terminal $J\alpha$ -extension (Figure 1, Supplementary Table S1A, S1B). While the N-cap region is relatively conserved, the Cterminal Jα-helix is variable in both, length and sequence. We previously reported structural and mutational studies on three of the slow and fast reverting *Pseudomonadaceae* short LOV proteins PpSB1-LOV, PpSB2-LOV and W619 1-LOV from Pseudomonas putida. 18,23,43,45,46,5

In the current study, we present the crystal structures of two Pseudomonadaceae short LOV SBW25-LOV and Pf5-LOV from proteins: Pseudomonas fluorescens SBW25 and fluorescens Pf-5.53 A comparative assessment of these structures and our previously reported *Pseu*domonadaceae short LOV crystal structures in the light, dark, and apo states reveal a highly conserved signaling mechanism among the LOV proteins of the Pseudomonadaceae family. As observed for the short LOV proteins of Pseudomonas putida KT2440, despite high sequence identity (\sim 73%), the SBW25-LOV and Pf5-LOV proteins show very different dark recovery kinetics of 1470 min and 3.6 min at 37 °C, respectively (Supplementary Table S1A, S1B). Interchanging certain nonconserved residues in a solvent channel lining the chromophore between the two proteins resulted in a correlated acceleration or deceleration of the dark recovery of the two proteins. Thus, due to their conserved sequence, structure, and signaling mechanism, as well as the ability to choose between slow and fast cycling LOV domains, the *Pseudomonadaceae* short LOV protein family offers a wide range of choices for synthetic biology applications such as the development of LOV-based optogenetic tools (reviewed in⁵⁴).

Results and Discussion

Uv-Vis spectroscopy, single crystal microspectrometry and dark recovery kinetics

The purified SBW25-LOV and Pf5-LOV proteins were obtained in chromophore loaded form, with HPLC analyses (Supplementary Table S2) revealing FMN as the predominately (>70%) bound flavin chromophore, which is in good agreement with previous reports. ^{23,41,45}

SBW25-LOV undergoes a photocycle similar to other LOV proteins, albeit with an extremely slow dark recovery. Complete dark recovery at 20 °C could not be achieved even after 16 h of observation. At 37 °C, however, an adduct-state lifetime (τ_{rec}) value of 1470 min was measured previously. The SBW25-LOV protein crystallized under permanent blue-light ($\lambda_{max} = 450$ nm) illumination (see Methods section). The UV-Vis absorption spectrum of protein crystals was measured to confirm that the protein is in the light state. For comparison, the UV-Vis absorption spectra of SBW25-LOV in solution, in the light and partially dark states are depicted in Figure 2(a). The crystal spectrum shown is identical to the light state spectrum of SBW25-LOV in solution, except for the higher intensity of the peak, which could be due to a higher protein concentration in a crystal (crowding) and the crystal orientation. The complete dark state could

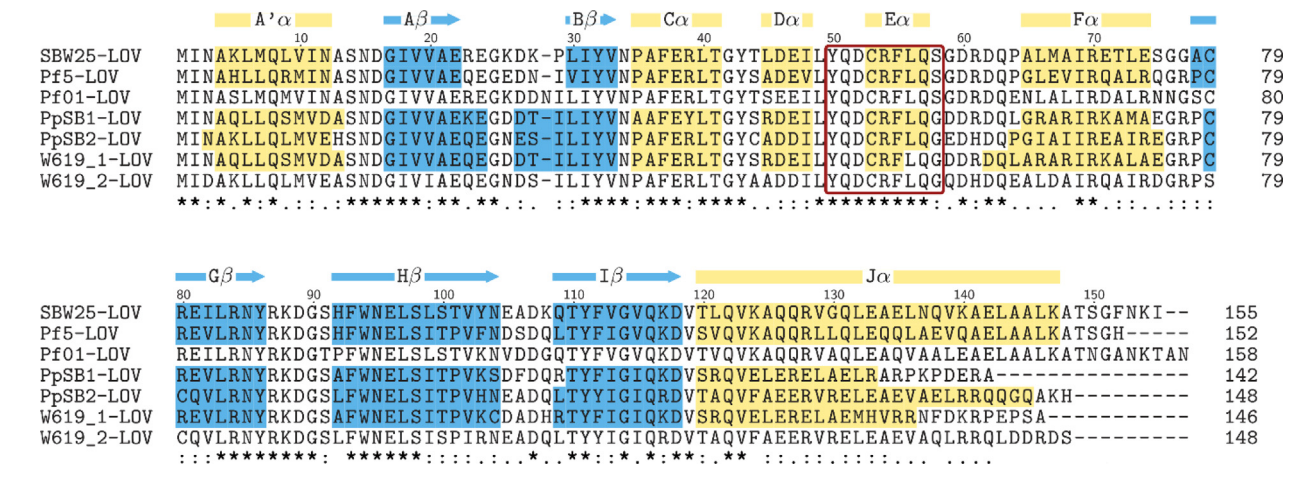


Figure 1. The sequence alignment of short LOV proteins from *P. putida* and *P. fluorescens*. The sequence alignment was generated with Clustal Omega. ⁵⁵ The secondary structure was assigned with the DSSP program from crystal structures, where helix (yellow) and strand (blue) are marked in the sequences. Secondary structure element labels are shown at the top. The asterisks in the bottom line of the alignment indicate identical residues in a given sequence position, while double dots and single dots refer to residues conserved to >70% and 50–70%, respectively. Sequence numbering for SBW25-LOV is shown at the top. The conserved Y(Q/R)DCRFLQG sequence motif, bearing the adduct forming cysteine, identified in *Pseudomonadaceae* LOV proteins is highlighted by a red box.

not be populated in solution due to the instability of the protein, as it undergoes proteolysis over such a long period of time. Nevertheless, the dark state spectrum showed characteristic peaks: three peaks in the region 400 nm–500 nm and broad peak at 365 nm, which originate from the bound flavin chromophore. Upon blue-light illumination, the covalent adduct is formed between the chromophore and the conserved cysteine residue leading to the loss of absorbance at 450 nm and the concomitant formation of a new broad peak with a maximum at around 390 nm.

Pf5-LOV is a short LOV protein originating from Pseudomonas fluorescens strain Pf-5 and a close homolog of SBW25-LOV (Figure 1). The spectrum of Pf5-LOV in the dark and light states showed characteristic absorption peaks, indicating a photocycle similar to that of other LOV proteins (Figure 2b). The crystals of Pf5-LOV protein grew under dark conditions, and UV-Vis spectrum of the crystals used for data collection confirmed their dark state (Figure 2b). The spectrum is similar to the dark state spectrum of Pf5-LOV in solution, except minor differences that might be related to the fact that spectra were measured at a temperature of 100 K instead of room temperature. In contrast to SBW25-LOV, Pf5-LOV has a shorter adduct state lifetime of 45.3 ± 0.7 mi n at 20 °C (Supplementary Figure S1), in general agreement with previous data measured at 37 °C (adduct lifetime of 3.6 ± 1.5 min), which indicated that the protein is fast cycling.4

Crystal structure of SBW25-LOV

Using the crystals obtained under continuous blue light conditions, we determined the structure of SBW25-LOV with a resolution of 1.6 Å in the P1 space group. The data collection and refinement statistics are listed in Table 1. The

previously published structures for other members of the *Pseudomonas* short LOV family such as PpSB1-LOV^{23,46}, PpSB2-LOV⁴⁵ and W619_1-LOV⁴³. The final atomic model in the asymmetric unit is a dimer, where the monomer subunits are related by a 2-fold non-crystallographic symmetry (Figure 3).

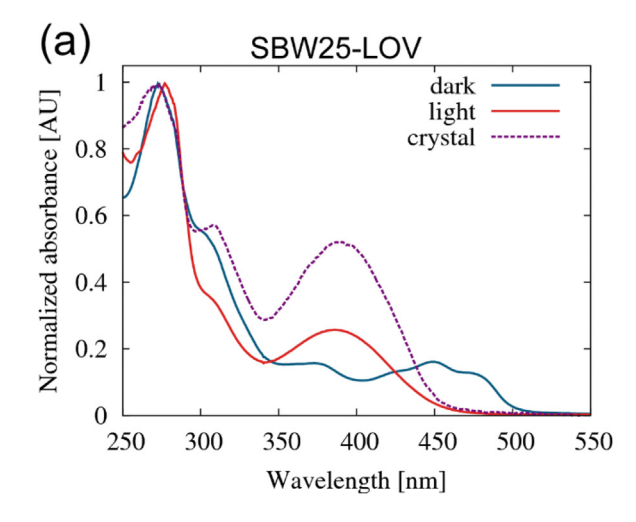
Well-defined electron density was observed for 148 residues in chain A and 150 in chain B, out of

structure revealed an overall fold similar to the

Well-defined electron density was observed for 148 residues in chain A and 150 in chain B, out of a total of 155 amino acids in the protein sequence. The superposition of the monomers demonstrates high similarity with a root mean square deviation (RMSD) of the C α -atom positions of 0.89 Å over residues 1–133 (Figure 3). In contrast, from residue 134 onwards, the positional differences in the J α -helix become more than 4 Å and were excluded from the RMSD calculation. Other differences between the two monomers are localized in the G β -H β loop and the A' α -helix, which are likely induced by crystal packing.

PISA analysis⁵⁷ of the SBW25-LOV dimer observed in the crystal structure revealed a calculated total buried surface area of 4157 Ų with a solvation energy gain of 37.1 kcal/mol upon dimer formation, indicating a stable dimer in solution. The dimer interface is stabilized by hydrophobic interactions in addition to hydrogen bonds and salt bridges (Table 2). The interfacial residues are predominantly located in the A' α -helix, J α -helix and are distributed throughout the β -strands. The sequence of the J α -helix shows characteristic heptad repeats leading to the coiled-coil-like interactions that contribute significantly to the interface (Figure 3).

The J α -helix of chain B shows a kink with an approximate angle of 26°, measured between the two vectors defined by the C α atoms of residues 125–128 and 128–131, using the HELANAL-Plus program. ⁵⁸ In comparison, chain A has a maximum



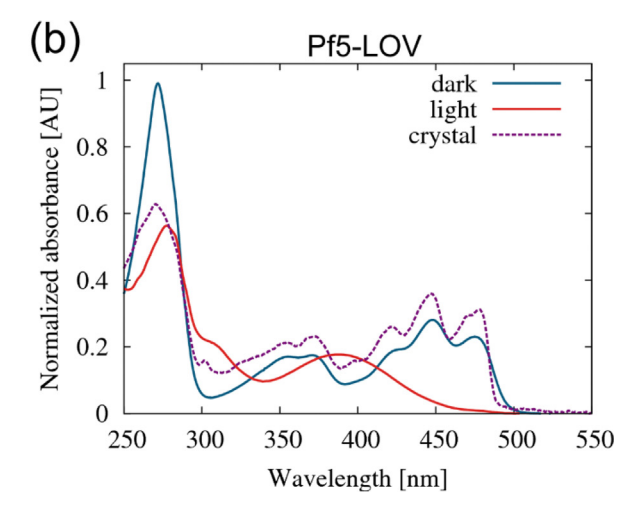


Figure 2. UV–Vis absorption spectra of SBW25-LOV (a) and Pf5-LOV (b) in solution and in crystal. The solution spectrum in the light (red) and partial dark states (blue) in solution are shown as solid lines, the spectrum of the protein crystal used for the structure determination is shown as a dashed line.

Table 1 Data collection and refinement statistics.

X-ray data	SBW25-LOV, light state PDB ID: 7YX0	Pf5-LOV, dark state PDB ID: 7R5N		
Beamline	ID23-2, ESRF	ID29, ESRF		
Detector	PILATUS 6 M	PILATUS 6 M		
Wavelength [Å]	0.873	0.976		
Resolution range [Å]	39.77–1.60 (1.63–1.60)*	48.12–3.45 (3.70–3.45)*		
Space group	(1.03–1.00) P1	(3.70–3.43) I4 ₁ 22		
Unit-cell a, b, c [Å]	36.26 42.44 51.74	148.7 148.7 200.79		
α, β, γ [°]	95.27 95.71 109.02	90 90 90		
Total reflections	125.311	72,313 (17255)		
Unique reflections	36,845 (1827)	15,076 (3526)		
Multiplicity	3.4 (3.4)	4.8 (4.9)		
Completeness [%]	97 (95.2)	99.5 (99.8)		
Mean $I/\sigma(I)$	5.0 (1.3)	9.0 (1.0)		
Wilson B-factor [Å ²]	19.56	155.21		
R-merge	0.093 (0.705)	0.081 (1.885)		
R-meas	0.11 (0.836)	0.091 (2.115)		
CC _{1/2}	0.992 (0.761)	0.997 (0.531)		
Refinement				
Resolution range [Å]	33.6–1.6	47.18–3.45		
0 1 1	(1.66–1.6)	(3.57–3.45)		
R-work	0.1882 (0.2249)	0.2152 (0.3481)		
R-free	0.2385 (0.2983)	0.2495 (0.3284)		
coordinate error (maxlikelihood based) [Å]	0.2	0.42		
Number of non-hydrogen atoms	2816	2460		
macromolecules	2569	2398		
Ligands	129	62		
Water	118	_		
Protein residues	316	300		
RMSD (bonds) [Å]	0.006	0.004		
RMSD (angles) [°]	0.79	0.76		
Ramachandran favored [%]	97.76	96.62		
Ramachandran outliers [%]	0	0		
Clashscore	3.12	8.02		
Average B-factor [Ų]	31.10	195.64		
macromolecules [Ų]	31.31	195.66		
ligands [Å ²]	25.07	194.76		
solvent [Ų]	33.17	_		

^{*} Statistics for the highest-resolution shell are shown in parentheses.

kink angle of only 9.6°. Interestingly, SBW25-LOV neither contains proline nor a specific sequence that is prone to induce an $\alpha\text{-helix}$ kink at this position. A possible significance of the kink in the context of signaling is discussed later in the manuscript.

Chromophore binding pocket in the crystal structure of SBW25-LOV

As shown in Figure 4, the FMN chromophore can clearly be identified in the $2mF_o\text{-}DF_c$ electrondensity map. This observation is consistent with the HPLC results for chromophore content analysis, with FMN being the dominant chromophore ($\sim\!71\%$). In previous structural studies, the continuous electron density and the bond distance of < 2.3 Å between the $S\gamma$ atom of the active site of the cysteine residue and the C4a atom of the FMN were used as indicators of the

presence of a covalent FMN-Cys bond, i.e., the light state of the LOV protein. In contrast, a noncontinuous electron density and a larger bond distance (>3.2 Å) suggests the dark state. In the SBW25-LOV crystal structure determined from the crystal grown under continuous light conditions, the electron density of individual atoms shows anisotropic distribution, such as those of FMN and surrounding residues Cys53, Gln57 and Leu97. Such an anisotropic distribution can, for example, be the consequence of the collective motions of the atoms or the result of an averaging across the different conformations present in the crystal. The electron density map shows a continuous density between the FMN-C4a atom and the Cys-Sy atom. In addition, two conformations of the Cys53 side chain were observed (Figure 4). For refinement, we modeled both the conformations of FMN- first, with planar ring as in the dark state

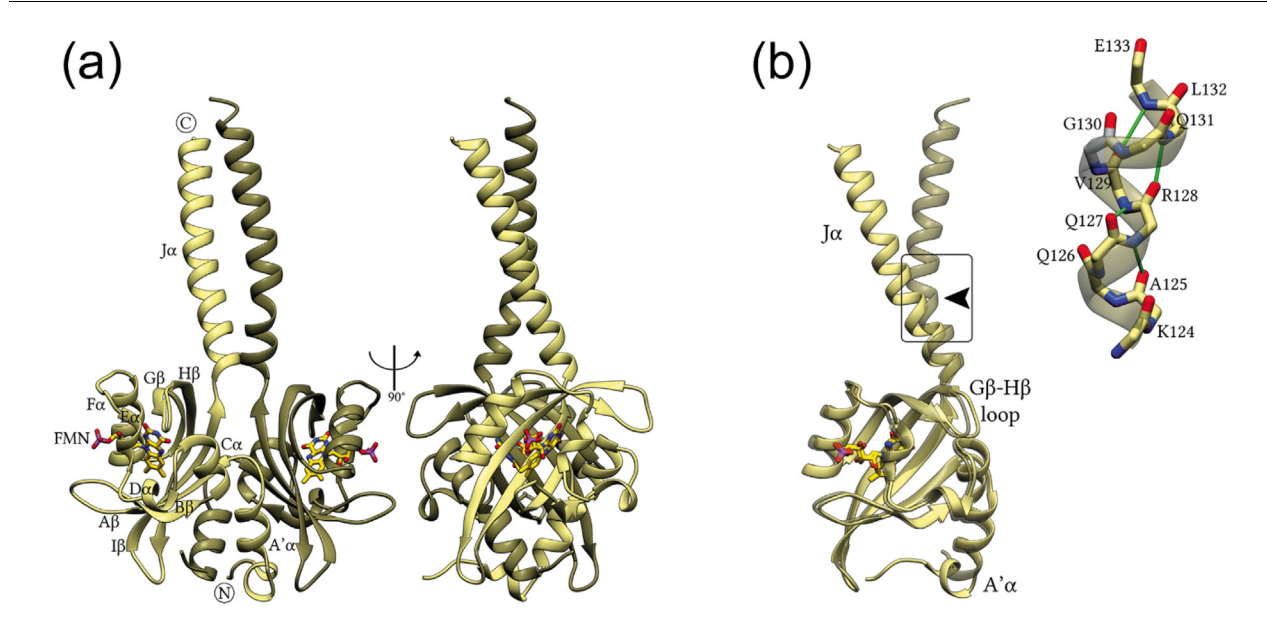


Figure 3. The crystal structure of the SBW25-LOV in the light state. The structure is represented as ribbons, where chains A and B are colored in light and dark shades of gold. FMN is shown as a stick model. (a) The dimer of SBW25-LOV observed in the crystal structure. (b) The superposition of the SBW25-LOV monomers by the core domain residues 17–117, which showed the differences in the G β -H β loop and the A' α , J α helices. After superposition, the RMSD of the C α atom positions is 0.89 Å over the residues 1–133. The residues at maximum kink of Chain B J α -helix, indicated by a box, are shown as sticks in the inset. The hydrogen bonds between backbone N and O atoms are shown as green lines.

Table 2 The interfacial residues of SBW25-LOV monomers in the dimer within the hydrogen bond distance of ≤3.2 Å.

Secondary structure element	Residue of chain A	Atom	Distance [Å]	Atom	Residue of chain B	Secondary structure element
Α'α	Gln8	NE2	3.1	0	lle2	_
Α'α	Ala13	0	2.7	OG	Ser100	Нβ
			2.8	OG	Ser100	Нβ
Α'α-Αβ Ιοορ	Asn15	ND2	3.1	OG	Ser98	Нβ
Α'α-Αβ Ιοορ	Asp16	OD1	3.0	NH1	Arg80	Gβ
			2.8	NH2	Arg80	Gβ
			2.9	OG	Ser98	Нβ
Gβ	Arg80	NH2	2.7	OD1	Asp16	Α'α-Αβ Ιοορ
Нβ	Glu96	OE1	2.9	NZ	Lys117	Ιβ
Нβ	Ser98	OG	2.8	OD2	Asp16	Α'α-Αβ Ιοορ
			2.8	ND2	Asn15	Α'α-Αβ Ιοορ
Нβ	Ser100	OG	2.8	0	Ala13	Α'α
$J\alpha$	Arg128	NE	2.9	OE2	Glu133	$J\alpha$
Jlpha	Arg128	NH2	2.9	OE2	Glu133	$J\alpha$

and second, non-planar ring as in the light state where the planarity in the ring system is disrupted by the sp3-hybridization of C4a atom which is involved in the FMN-cysteinyl adduct formation. For this, we used the FMN geometry optimized using quantum chemical calculations (QM) described in our previous report, 45 also due to the fact that atomic resolution experimental data is still missing for the geometry of the FMN-cysteinyl adduct where the FMN-C4a atom is sp3 hybridized. After refinement, the distance between the FMN-C4a and Cys53-S γ atoms was 2.02 Å (1.98 Å in chain B) and 3.52 Å (3.41 Å in chain B), corresponding to the FMN conformation in the light and dark states, respectively. The relative occupancies

between the light and dark states were 0.71 / 0.29 (0.43 / 0.57 in chain B). In previous studies reporting structures in the light state, this 'mixed' state observation was attributed to either a very rapid dark recovery rate and/or radiation damage from X-rays. $^{5.47,59}$ The recovery rate of SBW25 is extremely slow (with a $\tau_{\rm rec}$ value of 1470 min at 37 °C), and is not expected to affect dark recovery under cryogenic conditions, i.e., at 100 K during data acquisition, although we cannot completely rule this out due to lack of evidence. The UV–Vis absorption spectrum of the crystal showed that the chromophore was in the light state before X-ray irradiation, i.e. a covalent adduct was present, as evidenced by the absence of absorption at

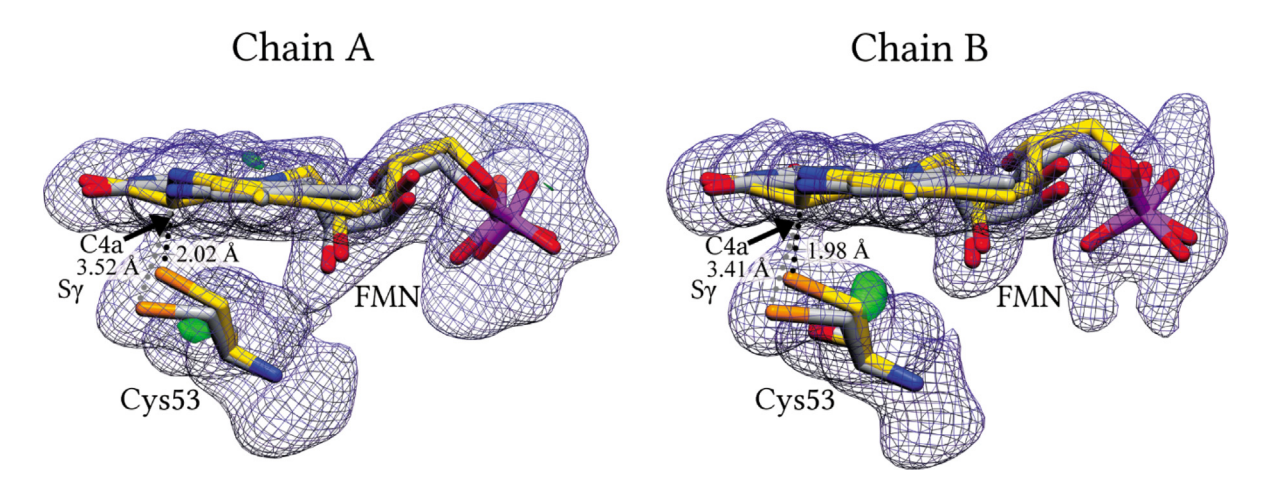


Figure 4. FMN electron density maps in the SBW25-LOV light state structure. Two conformations of the Cys53, and the "light state" and "dark state" FMN structures used in the refinement, representing the dark and light states are shown. The relative occupancies between the "light" and "dark" states were 0.71/0.29~(0.43/0.57~in~chain~B). $2mF_o-DF_c$ electron-density maps contoured at 1 RMSD are shown as a blue mesh. mF_o-DF_c difference maps contoured at $\pm 3~RMSD$ are shown as a transparent surface, where difference maps with positive values are colored green. FMN and the conserved Cys53 are shown as a stick model and colored by element: nitrogen, blue; oxygen, red; phosphorus, purple; sulfur, orange. The carbon atoms of "dark state" molecules are colored in grey and that of the "light state" in yellow.

450 nm and a distinct maximum at around 390 nm. In contrast, after X-ray irradiation during data collection, the UV-Vis spectrum of the crystal no longer showed a spectrum typical of the light state (Supplementary Figure S2), but instead, minor peaks appeared at around 450 nm, indicating at least partial disruption of the covalent FMN-Cys adduct caused by the radiation damage. This observation suggest that the obtained electron density map is likely an average between the light state with the intact covalent Cvs53-FMN-C4a (FMN) adduct and a conformation with locally disrupted adduct, that might be similar to the dark state. However, partial disruption of the adduct due to radiation damage is not expected to affect the large conformational changes in the tertiary and quaternary structure because the movements of the secondary structure elements are limited by the constraints of the crystal packing where the SBW25-LOV crystals formed under permanent blue light illumination.

Crystal structure of Pf5-LOV

The crystal structure of dark-adapted Pf5-LOV was determined up to a resolution of 3.45 Å in $I4_122$ space group. The data collection and refinement statistics are listed in Table 1. The asymmetric unit contains a homodimer, which is formed by monomers with a non-crystallographic 2-fold symmetry (Figure 5). The electron density map allowed observation of 149 of the 152 residues in chain A and all 152 residues in chain B. The superposition of the monomers shows their similarity with a root mean square deviation (RMSD) of 0.89 Å for the $C\alpha$ -atom positions over residues 1–139. Similar to the SBW25-LOV

structure, the J α -helix of chain B exhibits a kink with an angle of 26°, measured between the two vectors formed by the C α atoms of residues 125 to 128 and 128 to 131 with the HELANAL-Plus program. In comparison, chain A has maximum kink angle of 15.8°, which is higher than 9.6° observed in the equivalent chain in the crystal structure of SBW25-LOV.

The diffraction data of Pf5-LOV crystals showed a high relative Wilson B factor of 155 Å² (Table 1). The estimated solvent content of the protein crystal based on the Matthews probability was \sim 83%, which is high compared to a range between 40%-60% that is typical for protein crystals. Accordingly, the crystal had very loose packing with broad solvent channels. High values of the Wilson B factor are associated with a loss of detail in the electron density maps, and in this case, a combination of high solvent and lowresolution data resulted in an electron density map that was not well-defined, in which mostly residues truncated to the Cβ atom were modeled. requiring more precise Analysis atomic coordinates were therefore not performed for the Pf5-LOV structure model.

Comparative structural analysis highlights a conserved signaling mechanism in short LOV proteins of the Pseudomonas family

Based on structural studies of light and dark states of the *Pseudomonas putida* PpSB1-LOV and PpSB2-LOV protein dimers, we previously proposed a signaling mechanism in which light-induced changes in the chromophore pocket trigger rotation of the two protein chains relative to

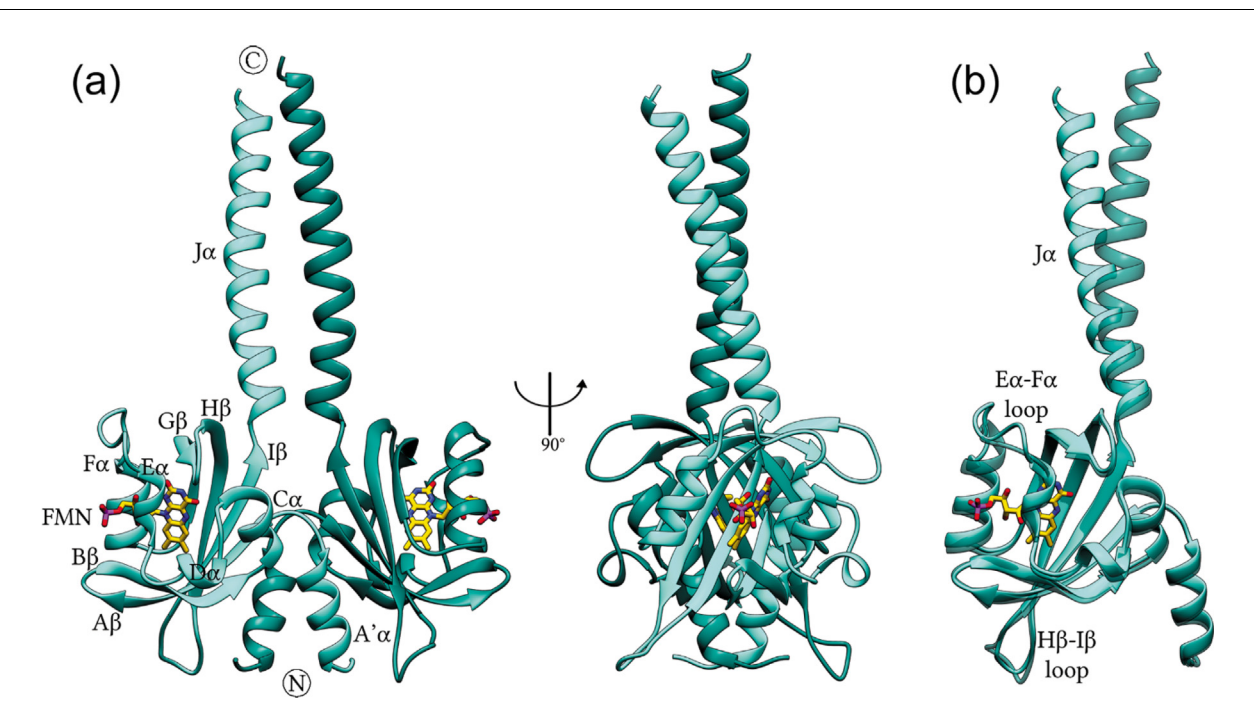


Figure 5. The crystal structure of Pf5-LOV in the dark state. The structure is represented as ribbons, where chains A and B are colored in light and dark shades of cyan. FMN is shown as a stick model. (a) The dimer of Pf5-LOV observed in the crystal structure. (b) The superposition of the Pf5-LOV monomers by the core domains residues 17–117, which showed the differences in the Hβ-Iβ and $E\alpha$ -Fα loops and the Jα helices. After superposition, the RMSD of the Cα atom positions is 0.89 Å over the residues 1–139.

each other, resulting in large movements in the Cterminal Jα-helices that relay the signal from the sensor to the associated effector domains. 45,46 Very similar structural conformations in the respective dark and light states, as well as the light-induced global conformational changes in both proteins, led us to speculate that this signaling mechanism could also be transferred to other structurally conserved short LOV proteins from different Pseudomonas species. Superposition of the two structures presented here, SBW25-LOV dimer in the light state and the Pf5-LOV dimer in the dark state resulted in a poor match (Figure 6c). This is consistent with studies on the dark and the light states of PpSB1-LOV and PpSB2-LOV, where the overall fold of short LOV proteins from Pseudomonas family reported in the current and our previous work is similar. 23,43,45,46

Next, we performed pairwise analysis of the short LOV protein structures in the light and dark conditions from the Pseudomonas (Table S3). Considerable differences are observed in the $J\alpha$ helices within the monomers of a dimer, so that caution is required when interpreting $J\alpha$ movement in the context of signaling. It is also worth noting that no crystal contacts were observed between the $J\alpha$ and $A'\alpha$ helices (Supplementary Figure S3). While $J\alpha$ and $H\beta$ - $I\beta$ loops are variable among LOV proteins of the Pseudomonas family, the core domain is quite conserved where most of the sequence differences can be identified in A' α , F α , the A β -B β

loop and the $H\beta$ -strand (Figure 1). The core domain residues (17-117)of equivalent monomers were superimposed as described previously. 45,46 The rotation values in Supplementary Table S3A reflect the degree of rotation required for molecule B to superimpose itself over its corresponding counterpart in the two structures. with molecules A initially superimposed. The larger rotation values between two structures indicates larger differences, for example, a \sim 15–25° rotation is observed between the dark and the light state structures of PpSB1-LOV. Please note that the values provided in Supplementary Table S3 are comparable and were obtained applying the same protocol for all. We observe a clear trend (Supplementary Table S3A), where the rotation angles between two structures in the light state ($\leq 5^{\circ}$) or dark state (≤7°) are relatively small compared to the rotation angles between a light and dark state $(11-29^{\circ}).$

The distances between the two subunits of a dimer were measured at three reference points: one, at the center of the core domains which was determined between the respective center-of-mass (COM) values (Figure 6d). We observe that this distance is comparatively smaller in the light state (\sim 26 Å) than in the dark state (\sim 30 Å), i.e. the core domains are located closer to each other. For the second and the third reference points, we selected residues 15 and 118 positioned at the N-and C-terminal ends of the core domain, both of which move apart in the light. Compared to the

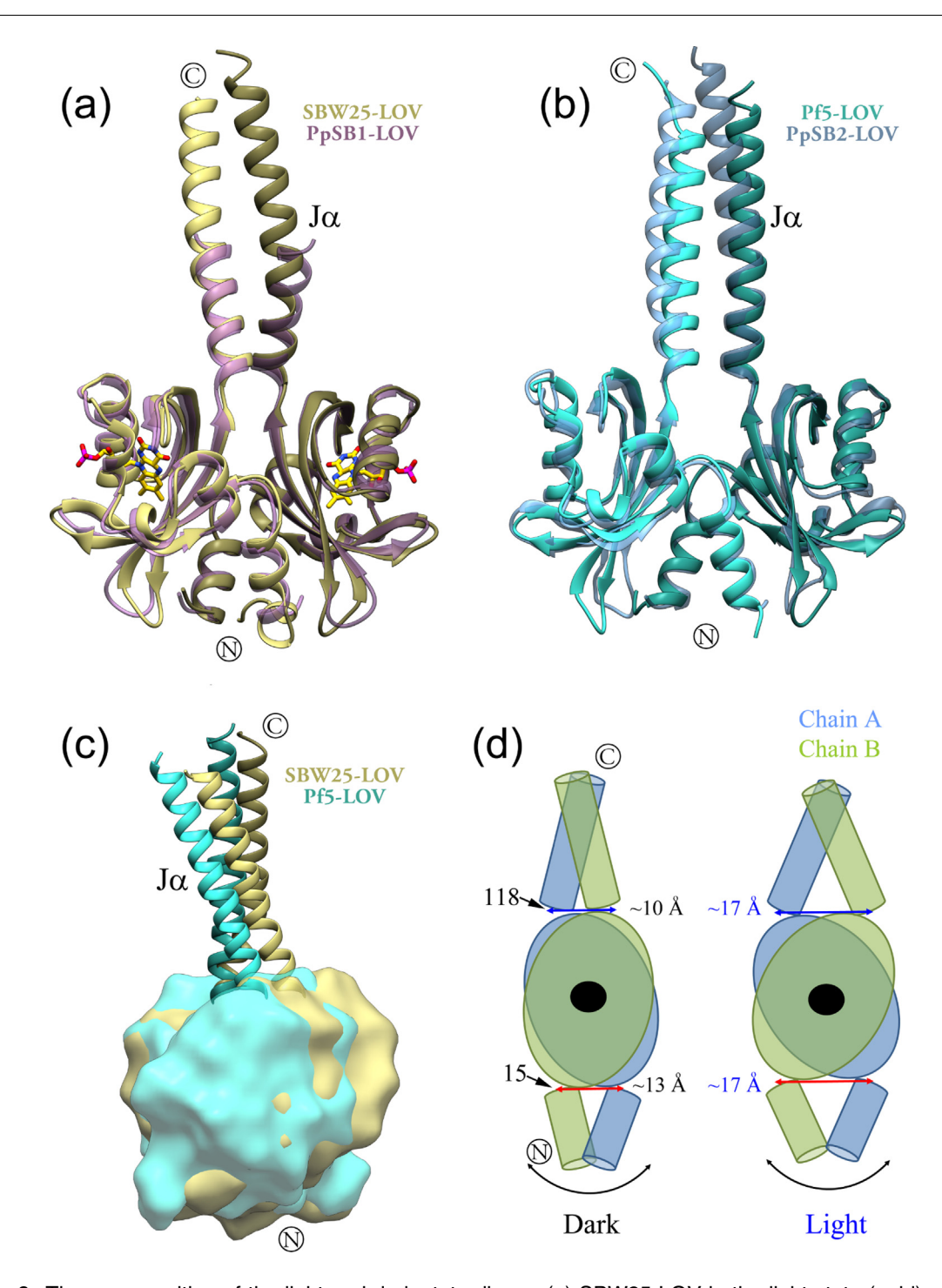


Figure 6. The superposition of the light and dark state dimers (a) SBW25-LOV in the light state (gold), and SB1-LOV in the light state (plum)(PDB ID 3SW1) are shown as ribbons, where chains A and B are colored in light and dark shades. (b) Pf5-LOV in the dark state (cyan), and SB2-LOV in the dark state (light blue)(PDB ID 7A6P). (c) SBW25-LOV in the light state (gold) and Pf5-LOV in the dark state (cyan). The panel shows superposition where LOV core domains are represented as surfaces, and J $_{\alpha}$ helices as ribbons to emphasize the dimer interface rotation. The RMSD between the core domain residues 17–117 of SBW25-LOV and Pf5-LOV is 1.1 Å and 0.9 Å for their A chains and B chains, respectively. (d) Cartoon representation of the dimer interface rotation observed between the dark and light structures when viewed from the side. The black circle indicates the center of mass (COM) of the core domain, and the curved arrows represent rotation between the two protein chains of a dimer. The straight double-headed arrows around amino acid residues 15 and 118 represent the distances between the two protein chains in the light and dark state dimers (Supplementary Table S3B).

dark state, we measured a \sim 7 Å increase in distance ($C\alpha$ - $C\alpha$) between 15–15 at the A' α -AB loops, and \sim 3 Å at 118–118 at the N-terminal end of the $J\alpha$ -helices (residues in italics are from the opposite subunit) (Supplementary Table S3B). The RMSD values and the Q-score are further parameters reflecting structural similarity. The Qscore varies between 0 (for completely dissimilar structures) and 1 (identical structures) and is a more objective indicator of the quality of the alignment than RMSD and N align alone. 57 Supplementary Table S3C shows a high Q-score (>0.7) for two randomly selected LOV structures, both in either the dark or light state, indicating general structural similarity. In contrast, the lower Q-score (<0.4) between two different LOV proteins- one in the dark and the other in the light state indicates structural differences.

Taken together, these observations suggest that the light-dependent global structural changes, such as rotation of the core domains relative to each other, increased distance at the N- and Cterminal junctions, are essentially identical among here studied short LOV proteins Pseudomonadaceae. Interestingly, SBW25-LOV light state dimer interface reveals the presence of a unique salt bridge K117 - E96 (Table 2), which was previously identified in molecular dynamics simulations studies on the light-adapted (adduct) state of PpSB1-LOV.60 In contrast, these interactions are absent in the simulations on the darkadapted state, as well as in the respective darkstate crystal structures that became available soon after. 46 The distances between K117 and E96 are >10 Å in the dark-adapted crystal structures. In contrast, the corresponding distance is >2.9 Å in light-adapted crystal structures of SBW25 (current study) and PpSB1-LOV. 23,46 Based on the molecular simulations. Bocola et al. proposed that the lightdependent reorientation of the conserved glutamine Q116 which flips its side-chain oxygen atom position impacts the salt-bridge network constituted by K117 (I β) and E96 (H β), stabilizing the light state dimer. Disruption of the salt bridge interaction in the dark state thus has an impact on the displacement of IB and HB strands (as suggested by the increased 118-118 distance in Supplementary Table S3B) which results in a correlated rotation of both LOV core domains and subsequently large movements in the C-terminal J α -helices. Similar results were also recently obtained in a theoretical study, which employed a Markov state model (MSM) combined with molecular dynamics (MD) simulations to investigate the signal transduction pathway of PpSB1-LOV. 61 In this work, in addition to the E96 - K117 salt-bridge network, the Q5-D105 interaction as well as the D16-R80 and D16-K117 interactions were deemed important for the light dependent dimer rearrangement. Previously, we reported the same in the comparative analysis of the crystal structures of PpSB1-LOV in the dark

and fully light-adapted states. 23,46 For example, a shift of the H β -I β loop by \sim 4 Å towards the N-cap helix A' α leads to an additional hydrogen bonding interaction between Q5 and D105 in the dark state. NMR data reported in the same study also indicated involvement of the A β -B β and H β -I β loops in the light-dependent dimerization of PpSB1-LOV. 46 Furthermore, an increase in the crossing angles between the N-terminal A' α -helices (40° to 64° in the light state) and the C-terminal J α -helices (26° to 48° in the light state) around the dimer axis was calculated in the crystal structures. 46 A similar extent of changes in the J α -J α and A' α -A' α crossing angles was observed in the molecular simulations work. $^{60-62}$

It is striking that the C-terminal $J\alpha$ -helix among the Pseudomonadaceae short LOV proteins is variable in both, sequence and length (Figure 1).41 Our structures for the short LOV proteins of the Pseudomonadaceae family demonstrate the role of Jahelices in dimerization of PAS/LOV domains. In multidomain LOV proteins, the $J\alpha$ -helices form the connecting link for signal transduction from the sensor to the effector domain. Due to their amphipathic character, these linkers are packed in coiled-coil αhelical structures to facilitate dimerization. In addition, the crystal structures show variations in the relative orientation and bending (presence of kinks) in the α-helical coiled-coil structure, raising the obvious question whether this is functionally relevant. In multidomain proteins, the bending of these long α-helices is likely to be involved in the signal transduction between the LOV sensor and the regulatory domain, such as a kinase domain. In a recent report, Rinaldi et al. reported the crystal structure of a full-length LOV histidine kinase (LOV-HK) from Brucella abortus in the light and dark states. 63 Lightinduced covalent bond formation between the FMN and the protein triggers a series of structural changes that result in concerted motion of the LOV domains, such as rotation relative to the central axis and an increase in distance between the two subunits at the junction of LOV domains and the coupled $J\alpha$ helices. This leads to a change in the coupling between the LOV domain and the $J\alpha$ helices and consequently to a change in the coiled-coil interactions. These structural changes are expected to impose conformational strain on the long linker helices, causing them to kink or bend, resulting in asymmetry in the structure. These results are consistent with observations in the short LOV dimers of Pseudomonadaceae family, and other LOV proteins. $^{46,64-66}$ MD simulations of the full-length SBW25-LOV structure remained stable overall during the 200-ns time course of the simulation, with more variation in RMSD due to the higher dynamics of the $J\alpha$ -helices (Supplementary Figure S4). The two J α -helices adopted distinct conformations during the simulation, with one of the helices being kinked (see snapshots of the trajectory in Supplementary Figure S4). We previously

observed a kink and super-twisting of the $J\alpha$ -helices in the PpSB2-LOV structure. 45 Superposition of the averaged model of PpSB2-LOV in the light state derived from MD simulation with the structure of SBW25-LOV shows the similarity of the two structures, including the location of the kink (Supplementary Figure S5). Using time-resolved X-ray scattering and electron-electron doubleresonance (ELDOR) spectroscopy, light-induced structural rearrangements such as splaying apart and relative rotation of the two monomers were identified in two previous reports on YF1, a chimeric protein generated by fusion of the Bacillus subtilis YtvA LOV photosensor domain and the histidine kinase module of FixL from Bradyrhizobium japonicum. 64-66 The authors proposed left-handed supercoiling of the coiled-coil $J\alpha$ linker helix as the structural mechanism by which signals are relaved from the sensor to the effector domain in the sensor histidine kinase. In a study on the full-length natural blue-light receptor LOV-HK, Rinaldi et al. postulated that the structural changes mentioned above in the LOV domain lead to a relaxation of strain in the tethered helical spine (composing the long α -helices), which triggers further asymmetric reactions over long distances in the dimer scaffold. This eventually leads to a severe kink in the DHp (dimerization and histidine phosphotransfer) helices of the HK domain, thereby activating the attached CA (catalytic and ATP binding) subdomain. 63 Given the recent observation that light signaling mediated by short-LOV proteins in several Pseudomonads depends on a downstream interaction with a Class II LitR-like transcriptional regulator (TR), 11 it is tempting to speculate that the interaction between the short LOV proteins and the transcriptional regulator occurs via the $J\alpha$ helix region and that structural changes imposed on the $J\alpha$ - $J\alpha$ interaction by LOV-LOV subunit rotation enable or prohibit TR binding. The differences in helix length and the $J\alpha$ dimer interaction among the Pseudomonadaceae short LOV proteins may thereby be due to an evolutionary adaptation to enable interaction with the respective cognate TRs in the cell.

In addition to the $J\alpha$ -helix, the short LOV proteins of *Pseudomonadaceae* contains an N-terminal A'α helix, which is part of the N-cap region (residues 1–16), at the dimer interface. The A' α helices are intertwined and partly cover the adjacent β scaffold of the LOV core (Figure 3). In our comparative structural analysis, significant lightinduced structural changes were observed in the N-terminal A' α -helices, which are evident from the increased distance between the $C\alpha$ atoms of residue 15-15 (Supplementary Table S3B) in the two subunits. In the PpSB1-LOV light structure, the A' α -helix is shorter by one residue, due to the unfolding of the A' α helix. ⁴⁶ This results in a change in the crossing angle, as was previously predicted by molecular simulations. 60 In a recent study, Zayner et al. showed that both, the N- and C-terminal

helices of AsLOV2 domain of Avena sativa Phototropin 1 are necessary for allosteric regulation of the phototropin kinase domain. 67 Phototropin 1 consists of two nonidentical LOV domains LOV1 and LOV2, and a serine-threonine kinase domain. The AsLOV2 domain is the most extensively studied model protein to study allostery and function among LOV proteins. The covalent adduct formation upon absorption of light in AsLOV2 results in the unfolding of the amino-terminal $A'\alpha$ helix and the carboxy-terminal Jα helix. Using Fourier-transform infrared difference spectroscopy, Zayner et al. show that deletion of the $A'\alpha$ helix abolishes the lightinduced unfolding of $J\alpha$, whereas extensions of the A' α helix lead to an attenuated structural change of $J\alpha$ helix. These results support the hypothesis that the α-helical linker domains on both. N- and C-termini are involved in the signal relay from the sensor to the effector domain.

Thus, in conclusion, the light-induced structural changes observed in the N- and C-terminal helices of the *Pseudomonadaceae* short LOV proteins, in analogy to the few known structures of LOV-effector fusion proteins, suggest that the N-terminal A' α -helices, in addition to the J α -helices, could serve as an interaction hotspot for a downstream signaling partner in the *Pseudomonadaceae* short LOV protein family. However, truncation studies combined with interaction assays¹¹ are needed to shed further light on these potential mechanisms.

Differences in the dark recovery kinetics between SBW25 and Pf5-LOV proteins

In order to understand the highly variable dark recovery kinetics of *Pseudomonas* short LOV proteins, we focused on SBW25-LOV and Pf5-LOV and introduced mutations targeted at mutually altering their recovery kinetics.

Mutual exchange mutations. SBW25-LOV and Pf5-LOV differ dramatically in their adduct lifetimes (1470 min vs 3.6 min at 37 °C), despite a sequence identity of ~73% (Supplementary Table S1B). The molecular basis for the significant differences in adduct-state decay kinetics among structurally conserved LOV domains is not fully understood. Performing a detailed site-directed mutagenesis study, we previously identified key amino acids on the A β -B β loop, the F α helix and a cluster of arginine residues that interact with the FMN phosphate moiety^{18,23,45} (see Table S1A for the list of adduct lifetimes). The arginine cluster, observed to be important for determining the slow and fast dark recovery of PpSB1-LOV and PpSB2-LOV from Pseudomonas putida is only partially conserved in SBW25-LOV and Pf5-LOV. While the arginine corresponding to R61 of PpSB1-LOV is conserved between SBW25-LOV and Pf5-LOV, the position of R66 of PpSB1-LOV is occupied by a leucine in both of the here studied

proteins. Thus, the arginine cluster observed to be important for tuning the dark recovery in the PpSB1- and PpSB2-LOV proteins, seems not to be decisive in case of SBW25-LOV and Pf5-LOV.

We therefore focused on the other previously identified hotspots for dark recovery tuning of Pseudomonadaceae short LOV proteins, the Aβ- $B\beta$ loop and the $F\alpha$ helix. We reasoned that mutations in these secondary structure elements will have an effect on the loop conformation thereby affecting the solvent accessibility to the bound chromophore, resulting in altered adduct stability and recovery kinetics. Interestingly, a sequence comparison of SBW25-LOV and Pf5-LOV showed again that the positions 23, 28 on $A\beta$ - $B\beta$ loop and 74 on $F\alpha$ helix, with all three residues lining a solvent channel to the chromophore, are not conserved in sequence. We thus generated a set of site-directed variants by mutually exchanging these residues between the two proteins individually as well as in different combinations (Table 3). For example, slow reverting SBW25-LOV harbors a Glu at position while Pf5-LOV has an Arg corresponding position. Consequently, introduced the E74R mutation in SBW25-LOV. introduced substitution The mutations are mutations between homologous, natural photoreceptors of Pseudomonas fluorescens, where no drastic changes in the overall structure of the resulting mutants are to be expected.

Dark recovery kinetics of all mutants reported in this study were measured at 30 °C by UV-Vis spectroscopy as described in the Methods section. The mutants resulting in a longer adduct state lifetime are referred to as decelerating mutants, while mutants that lead to a shorter adduct state lifetime are termed as accelerating mutants. For clarity, the accelerating and decelerating mutants in Table 3 are colored green and red, respectively. Amongst the single mutants, mutation of residue 28 showed a correlated deaccelerating effect in Pf5-LOV (~22fold for N28K), and an accelerating effect in SBW25-LOV (\sim 2.6 fold for K28N). The single mutation E74R in SBW25-LOV caused a marked acceleration of the recovery, while the mutual R74E mutation in Pf5-LOV only caused a moderate slow-down. Vice versa, the mutation at position 23 had only a moderate accelerating effect in SBW25-LOV but a much more pronounced accelerating effect in Pf5-LOV, ruling out correlating effects in both proteins. We next constructed the double (23/28, 23/74 and 28/74) and triple mutants (23/24/74). Interestingly, again the double and triple mutants that include the mutation of residue 28 showed more pronounced effect on the adduct lifetime, suggesting that the majority of the observed effect results from the mutation at position 28. This might be related to the fact the residue is directly lining the solvent channel, while the other tested residues are more proximal and hence have only modulating effects. Table 3 shows a general trend where substitution of the respective residues in the fast Pf5-LOV protein leads to a deceleration, whereas the corresponding mutants in the extremely slow SBW25-LOV protein lead to an acceleration of dark recovery. The exact degree of deceleration or acceleration is, however, incomparable for the two proteins, for example, deceleration observed in the Pf5-LOV triple mutant (23/24/74) was 30whereas the corresponding reverse exchange in SBW25-LOV showed an acceleration by only 2.5-fold. Nevertheless, a 2.5-fold acceleration for SBW25-LOV represents a remarkable change in dark recovery from \sim 117 h to ~47 h. Currently, we still lack understanding at the molecular level of all the factors affecting the kinetics of adduct recovery in the LOV domains. Both, others 19-22,24-27,29-31 and our previous studies^{18,23,28,45,52} have shown that the lifetime of the adduct state is not solely determined by individual residues or their positions in the chromophore pocket, but is the result of several contributing factors, such as hydrophobicity, cavity volume, interactions with (structured) water molecules. electrostatic interactions, etc. Residues in close proximity to the solvent channel attenuate the adduct decay rates by altering the stability of the N5 protonation state and hydrogen bonding to the active site flavin.25

Correlation between solvent accessibility and adduct lifetime. Probing the solvent-accessible cavity volume essentially reflects shape of the chromophore together with its solvent accessibility. To examine whether there is a relationship between solvent accessibility and dark recovery rate, we generated the solvent cavity by rolling a probe with a radius of 1.4 Å in SBW25-LOV, as shown in Figure 7. For comparison, we show the solvent-accessible cavities of a slowreverting PpSB1-LOV and a fast-reverting PpSB2-LOV protein with the dark recovery rates of 109 and 0.5 min at 37 °C.45 We observe a relation between the solvent accessibility and dark recovery rate, where the solvent cavity of SBW25-LOV is even more compact than that of PpSB1-LOV (Figure 7). In contrast, the solvent cavity is largest in the fast-reverting PpSB2-LOV protein. In the active site of SBW25-LOV, there is an intricate network of hydrogen bonds between residues Arg23, Lys28, Glu74, the structured water molecules 307 and 312, the chromophore FMN and the active site residues Cys53 and Asp52. Position 28 is at the Cterminal end of the Aβ-Bβ loop, which is occupied in the SBW25-LOV, PpSB1 and PpSB2-LOV proteins by Lys28, Thr28 and Ser28, respectively. Both, in dark and light states, residue 28 forms hydrogen bonds to the water molecule coordinated by the OH groups of the FMN ribityl chain. Unique to

Table 3 Dark recovery time constants of SBW25-LOV and Pf5-LOV and variants harboring respective mutations.

LOV proteins	SBW25- WT	SBW25- R23Q	SBW25- K28N	SBW25- E74R	SBW25- R23Q- K28N	SBW25- R23Q- E74R	SBW25- K28N- E74R	SBW25- R23Q- K28N- E74R
tau* [min]	7034	6188	2719	2188	3139	3582	2869	3390
st. dev*	185	152	157	137	340	147	40	504
fold change slower	1.0							
fold change faster	1.0	1.1	2.6	3.2	2.2	2.0	2.5	2.1
	Pf5-WT	Pf5- Q23R	Pf5- N <u>28</u> K	Pf5- R74E	Pf5- Q23R- N28K	Pf5- Q23R- R74E	Pf5- N <u>28</u> K- R74E	Pf5- Q23R- N <u>28</u> K- R74E
tau [min]	8.6	1.9	189	10.4	108.7	1.65	255	245.4
st. dev	0.13	0.01	1.18	0.04	5.7	0.09	1.15	1.55
fold change slower	1.0		22.1	1.2	12.7		29.8	28.6
fold change faster	1.0	4.5				5.2		

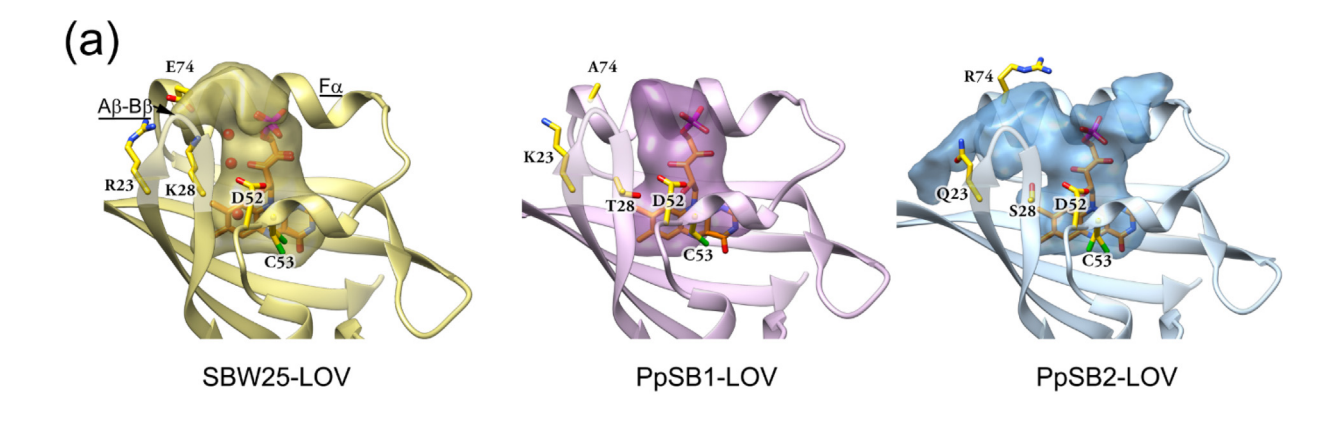
^{*}All measurements were performed at 30 °C; tau: dark recovery time; st. dev. standard deviation.

SBW25-LOV, Lys28 additionally interacts with the Glu74 on the F α -helix, closing the pocket and thereby hindering solvent access (Figure 7). In the sequence alignment with the related LOV proteins (Figure 1), only SBW25-LOV has this combination of Lys28 and Glu74 residues, while others have either Arg74 or Ala74 at the latter position. Moreover, Arg23 in SBW25-LOV is also located within the hydrogen bonding distance to Glu74, which allows for even better closure of the pocket with respect to the solvent (Figure 7).

Due to loss of details on the side chain conformations in Pf5-LOV structure, we did not solvent-accessible generate its cavity. Nevertheless, the above-mentioned hypothesis appears to be valid. As in PpSB2-LOV, Pf5-LOV has an identical combination of the Arg74 and Gln23 residues that are arranged in a similar manner. Phe112 instead of Tyr112 residue prevents the hydrogen bonding to Gln23, as seen previously in PpSB2-LOV. 45 Analogous to PpSB2-LOV, such sequence differences between Pf5-LOV and SBW25-LOV may account for the faster dark recovery of Pf5-LOV, suggesting that solvent accessibility to the FMN ring system correlates with adduct lifetimes.

In our previous work, MD simulations on PpSB2-LOV and PpSB1-LOV proteins under dark and light conditions indicated a correlation between increased protein dynamics and a faster dark recovery. 45 Here, we performed a 200-ns MD simu-

lation for SBW25-LOV in the light state using the crystal structure of SBW25-LOV in the light state as the initial structure (see details in the Methods section). The residue-resolved root-mean-square fluctuation (RMSF) of core domain residues 17-119 of SBW25-LOV were compared with those of PpSB1-LOV and PpSB2-LOV in the light states (Figure 7b). The overall RMSF of the main chain atoms (N, C, O, and C α) remained similar for most of the structure in all three LOV proteins (Supplementary Figure S4, panel a). However, lower RMSF values were observed in some regions of SBW25-LOV. For example, the $A\beta$ - $B\beta$ loop becomes more rigid in SBW25-LOV. In addition, the presence of the above-mentioned hydrogen-bond interactions of Lys28 and Arg23 with Glu74 (on the $F\alpha$ -helix) also stabilizes the Aβ-Bβ loop. In fact, RMSF values are lower for the side chains of these residues in the $A\beta$ - $B\beta$ loop and the C-terminal part of the $F\alpha$ -helix when compared to those of PpSB2-LOV and PpSB1-LOV (Supplementary Figure S4a). Both, the main chain and side chain atoms of the residues showed lower RMSF values. The $H\beta\text{-I}\beta$ loop in SBW25-LOV is more rigid, which may be related to the sequence divergence observed even among homologous short LOV proteins shown in the sequence alignment in Figure 1. Please note that, the medium/low resolution nature of the Pf5-LOV structure render MD simulations of this protein difficult, since any imprecisions in the structure of Pf5-LOV, would strongly influence the outcome of the



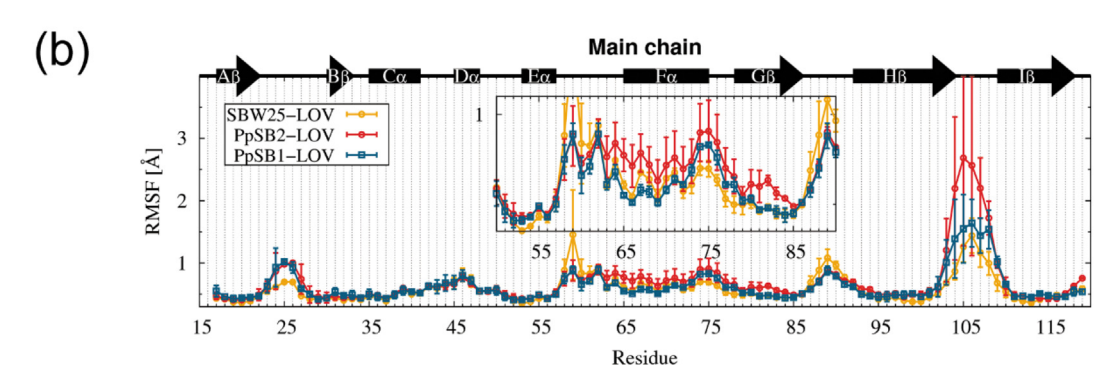


Figure 7. (a) Solvent-accessible cavities of the SBW25-LOV (gold), PpSB1-LOV (plum) (PDB ID: 5J3W) and PpSB2-LOV (blue) (PDB ID: 7A6P). The figure shown was generated with the UCSF Chimera software. (b) Residue-resolved RMSF of MD simulation of the main chain atoms of SBW25-LOV, PpSB2-LOV and PpSB1-LOV in the light states. The bars indicate the values of two monomers, whereas the points indicate their average. The secondary structure elements of SBW25-LOV are shown as arrows for strands and rectangles for helices. Secondary structure assignment was done with the DSSP program for the SBW25-LOV crystal structure.

MD simulation, and the timescales of classical MD simulations for a protein of this size cannot access the times necessary for convergence to its lower/correct energy state/structure.

Conclusions

In the present work, the crystal structures of two Pseudomonadaceae short LOV proteins are presented in the fully light-adapted state (SBW25-LOV) and the dark state (Pf5-LOV). Both proteins are short full-length LOV proteins that exhibit very different dark recovery rates of 1470 min and 3.6 min at 37 °C, respectively. Comparison of the respective structures, with previously reported dark and light state structures of homologues proteins⁴⁶ and previous MD simulations⁶⁰ highlight a conserved signaling mechanism for the short LOV protein family of Pseudomonadaceae. Bluelight illumination hereby results in subtle structural rearrangements in proximal amino acids including the 'flipping' glutamine 116 (IB) and the H-bonding network between residues of H β , I β , A β and A' α -Aβ loop. These rearrangements initiate global changes such as an increase in overall rigidity,

and rotation of the two domains relative to each other, causing large movements in the J α -helices that might relay the signal from the sensor to potential effector proteins, recently shown to be Class II LitR-like transcriptional regulators. In contrast to our previous studies, the much longer J α -helices of SBW25-LOV and Pf5-LOV show bending, with a more pronounced asymmetry observed in the light state. The motion of the helices can be described as supercoiling, which is consistent with other two-component LOV proteins as well as LOV-histidine kinases. To-75 Simultaneously, structural changes such as unfolding and increased distance between the A' α helices in the N-termini is also suggestive of their role in signaling.

To investigate the remarkable difference in dark recovery rates of the two homologous *Pseudomonadaceae* short LOV proteins, we introduced single, double and triple mutations where we exchanged the non-conserved amino acids from slow-reverting SBW25-LOV into a fast-reverting Pf5-LOV and *vice versa*. The selected residues show higher dynamics in the MD simulations and were expected to influence the solvent accessibility to the chromophore, as they

are located at the structural elements that form the entrance and exit of the solvent channel. The dark recovery kinetics of the resulting mutants could largely be reversed, suggesting a correlation between the solvent accessibility and the adduct lifetime.

The here presented results significantly broaden our understanding of the light-induced structural transitions, signaling mechanism and the dark recovery process in LOV proteins. This knowledge will have important implications for the design and development of LOV-based optogenetic tools. In this respect, the comparative analysis of structurally similar homologous short LOV proteins from the *Pseudomonadaceae* family with a wide range of dark recovery rates (from seconds to several days) provides a unique tool for developing LOV-based optical tools with finetuned signaling behavior (on/off kinetics).

Materials and Methods

Heterologous gene expression

The Pseudomonas fluorescens Pf5 and SBW25 LOV genes encoding LOV proteins SBW25-LOV and Pf5-LOV (UniProt entries C3K1W0 for SBW25-LOV, Q4KI48 for Pf5-LOV) were cloned as described previously.⁴¹ In brief, each of the constructs possessing an N-terminal hexahistidine tag (tag sequence: MGSSHHHHHHHSSGLVPRGSH), cloned in pET28a+ (Merck, Darmstadt, Germany) as expression vector, were expressed in E. coli BL21 (DE3). Autoinduction (AI) media⁷⁶ was prepared with Terrific Broth medium (X972; Carl-Roth, Karlsruhe, Germany) and supplemented with 50 μm riboflavin (A6279; AppliChem GmbH, Darmstadt, Germany), 50 µg/mL kanamycin and for induction, 0.5 g/L glucose, and 20 g/L lactose. Overexpression was carried out in 250 mL AI media cultures for 3 h at 37 °C. Afterwards, the incubation temperature was changed to 30 °C and the cells were incubated for 24 h with constant agitation at 110 rpm.

Protein purification

Both the LOV proteins were purified by using immobilized metal affinity chromatography (IMAC) as described previously. 41,45 The fractions containing purified protein obtained from IMAC were pooled, and the imidazole containing elution buffer was exchanged with the storage buffer [10 mm Tris pH 8.0, 10 mm NaCl], using ÄKTA pure FPLC system (GE Healthcare, Buckinghamshire, UK) with an HiPrep 26/10 Desalting column as per standard protocol. The eluted protein fractions were pooled, supplemented with 3 mM Tris(2-carboxyethyl) phosphine (TCEP), and concentrated by ultrafiltration using Vivaspin centrifugal concentrator units (molecular mass cutoff: 10 kDa) (Sigma-Aldrich; St. Louis, MO, USA).

Chromophore content and loading

The chromophore loading and the chromophore content quantification for both SBW25-LOV and Pf5-LOV were performed by UV–Vis spectroscopy and high-performance liquid chromatography (HPLC) as described previously.⁴⁵

Spectroscopic techniques

UV/Vis Spectroscopy measurements were carried out with Shimadzu UV-1800 а (Shimadzu, Kyoto, Japan) as spectrometer described previously. 45 Due to the very slow dark recovery kinetics of SBW25, we performed all dark recovery measurements at both 20 °C and 37 °C. For a direct comparison with Pf5-LOV, these measurements were performed at 30 °C for both the proteins. The sample was illuminated for at least 30 s using a blue-light (λ max = 450 nm) emitting LED with a radiant power of 50 mW (Luxeon Lumileds; Phillips, Aachen, Germany) to generate the respective light states. Dark recovery kinetics were then measured from the illuminated sample as described previously.41 The absorbance recovery at 475 nm was recorded as a function of time. The absorbance data were plotted against time with the Gnuplot program and fitted using a single exponential decay function. All measurements were done in triplicate.

Protein crystallization

The purified proteins SBW25-LOV and Pf5-LOV were concentrated to 8 and 15 mg/mL, respectively. Crystallization experiments were performed using the vapor diffusion method in 96well sitting-drop plates, with a drop size of 1.8 μL (0.9 μL purified protein plus 0.9 μL reservoir solution) against 70 µL of the reservoir solution. SBW25-LOV crystallized at 21 °C continuous light conditions where the plates were constantly illuminated with blue-light LED arrays $(\lambda_{max} = 450 \text{ nm}, \text{ Luxeon Lumileds}, \text{ Phillips},$ Aachen, Germany), with the reservoir containing 10%-12% PEG 3350, 0.1 M MES (pH 6.0-6.3). Pf5-LOV crystallized at 14 °C under dark conditions where the plates were kept wrapped in aluminum foil, with the reservoir containing 1.0 M- $1.2 \text{ M} (NH_4)_2SO_4$, 0.1 M MES (pH 6.0–6.3). Prior to cryocooling, 25% PEG 3350 (v/v) and 25% glycerol (v/v) were added in small steps (\sim 5%) to the SBW25 and Pf5-LOV crystals, respectively.

Single crystal microspectrometry

UV-Vis absorbance spectra of cryo-cooled crystals at 100 K were recorded in the wavelength range 250-700 nm using a microspectrometer at the beamline ID29S at ESRF (Grenoble, France) as described previously. The spectra of protein crystals were measured both, before and after X-ray exposure during data collection.

Data collection and structure determination

Single crystals were mounted in loops and flash frozen with gaseous nitrogen at a temperature of 100 K. All the steps for Pf5-LOV crystals, including data acquisition at the beamline, were performed under red-light conditions. X-ray diffraction data at 100 K were recorded at the ESRF beamlines ID23-2⁷⁸ and ID29⁷⁹ at Grenoble, France. The respective wavelengths and corresponding detector types of each beamline are listed in Table 1. The strategy for data collection was determined using the BEST program to reduce potential radiation damage from the beam while maintaining data collection as complete as possible.80 Data processing was performed using the XDS program⁸¹ and AIMLESS (part of the CCP 4 package).82 The initial phases were determined by molecular replacement using the program MOL-REP (CCP4 package). The search models for SBW25 and Pf5-LOV structures were based on the crystal structures of PpSB1-LOV (light state: PDB ID: 3SW1) and PpSB1-LOV (dark state: PDB ID: 5J3W), respectively. The SBW25 protein crystals obtained under blue light exhibit a triclinic crystal form and have space group P1 with diffraction up to 1.6 Å. For Pf5-LOV in the dark state, the tetragonal crystal form with space group 14,22 diffracted only up to 3.45 Å, with a high relative Wilson B factor (see Table 1) as a result of very loose crystal packing with high solvent content. Both the crystals have two molecules per asymmetric unit that are related by a two-fold NCS symmetry, i.e. are homodimers. The models described were further improved with several cycles of refinement using the program PHENIX⁸³ and manual rebuilding using the COOT graphics program.⁸⁴ Data collection and refinement statistics are listed in Table 1.

Molecular dynamic simulations

The light state dimer structure of SBW25-LOV (current work) was used as the initial model for the MD simulations, performed with help of GROMACS 5.1 software⁸⁵ using the AMBER-99SB-ILDN force field.86 Water, ions, and ligands except FMN were removed from the structure. The topology and partial charges of FMN-cysteine adduct were used from our previous study. 45 The models were solvated in a periodic box (with \geq 12 Å distance from any protein atom to the edge of the box) with TIP3P water molecules, and neutralized at a 150 mM NaCl concentration. The systems were energy-minimized with the steepest descent method followed by the conjugatedgradient method, and afterwards equilibrated at temperature of 298 K and 1 bar pressure. Cut-off for the electrostatic interaction with Particle Mesh Ewald algorithm⁸⁷ was 10 Å and that for the shortrange Van der Waals interactions was also 10 Å. The simulation time step was 2 fs and the trajectories were saved every 10 ps. The light state simulations for SBW25-LOV were run for 200 ns.

Graphical representation

Unless otherwise indicated, figures were generated with UCSF Chimera software, ⁶⁹ Molscript⁸⁸ and Raster3D⁸⁹ using secondary structure assignments as given by the DSSP program. ⁵⁶ UV–Vis spectra were plotted with the Gnuplot program. ⁹⁰

Accession Numbers

Atomic coordinates and structure factors for SBW25-LOV and Pf5-LOV were deposited in the Protein Data Bank (https://www.rcsb.org) under PDB IDs 7YX0 and 7R5N, respectively.

CRediT authorship contribution statement

Vladimir Arinkin: Conceptualization, Data curation. Formal analysis, Investigation, Methodology, Validation, Visualization, Writing -Joachim original draft. Granzin: Conceptualization, Formal analysis, Investigation, Supervision, Validation, Visualization. Karl-Erich Jaeger: Formal analysis, Funding acquisition, Resources. Dieter Willbold: Formal analysis, Resources. Ulrich Krauss: Formal analysis, Methodology, Visualization, Writing - review & editing. Renu Batra-Safferling: Conceptualization, Data curation, Formal analysis, Funding acquisition, Investigation, Methodology, Project administration, Supervision, Validation, Writing – original draft, Writing – review & editing.

DECLARATION OF COMPETING INTEREST

The authors declare that they have no known competing financial interests or personal relationships that could have appeared to influence the work reported in this paper.

Acknowledgements

This work was supported by grants from the Federal Ministry of Education and Research (Project OptoSys, FKZ 031A16).

The X-ray diffraction experiments were performed on the beamlines ID23-2 and ID29 at the ESRF (Grenoble, France). We are grateful to local contact persons at the ESRF for providing help in using beamline. Additionally, we are thankful to Dr. David von Stetten for the support on ID29S beamline for microspectrometry measurements.

Appendix A. Supplementary data

Supplementary data to this article can be found online at https://doi.org/10.1016/j.jmb.2024. 168458.

Received 11 July 2023; Accepted 23 January 2024; Available online 26 January 2024

Keywords:

LOV domain; flavoprotein; short LOV; PAS domain; photocycle

† Current address: University of Geneva, Department of Molecular Biology, 30 quai Ernest-Ansermet 1211, Geneva 4, Switzerland.

Abbreviations:

FMN, flavin mononucleotide; LOV, light-oxygen-voltage; PAS, Per-ARNT-Sim; Pf, *Pseudomonas fluorescens*; Pp, *Pseudomonas putida*

References

- Ponting, C.P., Aravind, L., (1997). PAS: a multifunctional domain family comes to light. Curr. Biol. 7, R674–R677.
- Möglich, A., Yang, X., Ayers, R.A., Moffat, K., (2010). Structure and function of plant photoreceptors. *Annu. Rev. Plant Biol.* 61, 21–47.
- Kottke, T., Heberle, J., Hehn, D., Dick, B., Hegemann, P., (2003). Phot-LOV1: photocycle of a blue-light receptor domain from the green alga Chlamydomonas reinhardtii. *Biophys. J.* 84, 1192–1201.
- Crosson, S., Moffat, K., (2002). Photoexcited structure of a plant photoreceptor domain reveals a light-driven molecular switch. *Plant Cell* 14, 1067–1075.
- Fedorov, R., Schlichting, I., Hartmann, E., Domratcheva, T., Fuhrmann, M., Hegemann, P., (2003). Crystal structures and molecular mechanism of a light-induced signaling switch: The Phot-LOV1 domain from Chlamydomonas reinhardtii. *Biophys. J.* 84, 2474–2482.
- Yee, E.F., Diensthuber, R.P., Vaidya, A.T., Borbat, P.P., Engelhard, C., Freed, J.H., Bittl, R., Möglich, A., Crane, B. R., (2015). Signal transduction in light-oxygen-voltage receptors lacking the adduct-forming cysteine residue. *Nature Commun.* 6, 10079.
- Dietler, J., Gelfert, R., Kaiser, J., Borin, V., Renzl, C., Pilsl, S., Ranzani, A.T., Garcia de Fuentes, A., et al., (2022). Signal transduction in light-oxygen-voltage receptors lacking the active-site glutamine. *Nature Commun.* 13, 2618.
- 8. Jones, M.A., Feeney, K.A., Kelly, S.M., Christie, J.M., (2007). Mutational analysis of phototropin 1 provides insights into the mechanism underlying LOV2 signal transmission. *J. Biol. Chem.* **282**, 6405–6414.
- Swartz, T.E., Tseng, T.S., Frederickson, M.A., Paris, G., Comerci, D.J., Rajashekara, G., Kim, J.G., Mudgett, M.B., et al., (2007). Blue-light-activated histidine kinases: twocomponent sensors in bacteria. *Science* 317, 1090–1093.

- Chen, C.H., DeMay, B.S., Gladfelter, A.S., Dunlap, J.C., Loros, J.J., (2010). Physical interaction between VIVID and white collar complex regulates photoadaptation in Neurospora. P. Natl. Acad. Sci. USA 107, 16715–16720.
- Maruyama, T., Sumi, S., Kobayashi, M., Ebuchi, T., Kanesaki, Y., Yoshikawa, H., Ueda, K., Takano, H., (2022). Class II LitR serves as an effector of "short" LOVtype blue-light photoreceptor in Pseudomonas mendocina. Sci. Rep. 12, 21765.
- Bannister, S., Bohm, E., Zinn, T., Hellweg, T., Kottke, T., (2019). Arguments for an additional long-lived intermediate in the photocycle of the full-length aureochrome 1c receptor: a time-resolved small-angle X-ray scattering study. Struct. Dyn. 6, 034701
- Röllen, K., Granzin, J., Batra-Safferling, R., Stadler, A.M., (2018). Small-angle X-ray scattering study of the kinetics of light-dark transition in a LOV protein. *PLoS One* 13, e0200746.
- 14. Chaudhari, A.S., Chatterjee, A., Domingos, C.A.O., Andrikopoulos, P.C., Liu, Y., Andersson, I., Schneider, B., Lorenz-Fonfria, V.A., et al., (2023). Genetically encoded non-canonical amino acids reveal asynchronous dark reversion of chromophore, backbone, and side-chains in EL222. Protein Sci. 32, e4590.
- Hart, J.E., Sullivan, S., Hermanowicz, P., Petersen, J., Diaz-Ramos, L.A., Hoey, D.J., Labuz, J., Christie, J.M., (2019). Engineering the phototropin photocycle improves photoreceptor performance and plant biomass production. *PNAS* 116, 12550–12557.
- Pudasaini, A., Shim, J.S., Song, Y.H., Shi, H., Kiba, T., Somers, D.E., Imaizumi, T., Zoltowski, B.D., (2017). Kinetics of the LOV domain of ZEITLUPE determine its circadian function in Arabidopsis. *Elife* 6
- Dasgupta, A., Chen, C.H., Lee, C., Gladfelter, A.S., Dunlap, J.C., Loros, J.J., (2015). Biological significance of photoreceptor photocycle length: VIVID photocycle governs the dynamic VIVID-white collar complex pool mediating photo-adaptation and response to changes in light intensity. *PLoS Genet.* 11, e1005215.
- Jentzsch, K., Wirtz, A., Circolone, F., Drepper, T., Losi, A., Gärtner, W., Jaeger, K.E., Krauss, U., (2009). Mutual exchange of kinetic properties by extended mutagenesis in two short LOV domain proteins from Pseudomonas putida. *Biochemistry* 48, 10321–10333.
- Losi, A., Kottke, T., Hegemann, P., (2004). Recording of blue light-induced energy and volume changes within the wild-type and mutated phot-LOV1 domain from Chlamydomonas reinhardtii. *Biophys. J.* 86, 1051–1060.
- Raffelberg, S., Mansurova, M., Gärtner, W., Losi, A., (2011). Modulation of the photocycle of a LOV domain photoreceptor by the hydrogen-bonding network. *J. Am. Chem. Soc.* 133, 5346–5356.
- Tang, Y., Cao, Z., Livoti, E., Krauss, U., Jaeger, K.E., Gartner, W., Losi, A., (2010). Interdomain signalling in the blue-light sensing and GTP-binding protein YtvA: a mutagenesis study uncovering the importance of specific protein sites. *Photochem. Photobiol. Sci.: Official J. Eur. Photochem. Assoc. Eur. Soc. Photobiol.* 9, 47–56.
- Zoltowski, B.D., Nash, A.I., Gardner, K.H., (2011).
 Variations in protein-flavin hydrogen bonding in a light, oxygen, voltage domain produce non-Arrhenius kinetics of adduct decay. *Biochemistry* 50, 8771–8779.
- 23. Circolone, F., Granzin, J., Jentzsch, K., Drepper, T., Jaeger, K.E., Willbold, D., Krauss, U., Batra-Safferling,

- R., (2012). Structural basis for the slow dark recovery of a full-length LOV protein from Pseudomonas putida. *J. Mol. Biol.* **417**, 362–374.
- Brosi, R., Illarionov, B., Mathes, T., Fischer, M., Joshi, M., Bacher, A., Hegemann, P., Bittl, R., et al., (2010). Hindered rotation of a cofactor methyl group as a probe for proteincofactor interaction. *J. Am. Chem. Soc.* 132, 8935–8944.
- Christie, J.M., Corchnoy, S.B., Swartz, T.E., Hokenson, M., Han, I.S., Briggs, W.R., Bogomolni, R.A., (2007). Steric interactions stabilize the signaling state of the LOV2 domain of phototropin 1. *Biochemistry* 46, 9310–9319.
- Zoltowski, B.D., Vaccaro, B., Crane, B.R., (2009).
 Mechanism-based tuning of a LOV domain photoreceptor. *Nature Chem. Biol.* 5, 827–834.
- Alexandre, M.T., Arents, J.C., van Grondelle, R., Hellingwerf, K.J., Kennis, J.T., (2007). A base-catalyzed mechanism for dark state recovery in the Avena sativa phototropin-1 LOV2 domain. *Biochemistry* 46, 3129–3137.
- Fettweiss, T., Rollen, K., Granzin, J., Reiners, O., Endres, S., Drepper, T., Willbold, D., Jaeger, K.E., Batra-Safferling, R., Krauss, U., (2018). Mechanistic basis of the fast dark recovery of the short LOV protein DsLOV from dinoroseobacter shibae. *Biochemistry* 57, 4833–4847.
- 29. Pennacchietti, F., Abbruzzetti, S., Losi, A., Mandalari, C., Bedotti, R., Viappiani, C., Zanacchi, F.C., Diaspro, A., et al., (2014). The dark recovery rate in the photocycle of the bacterial photoreceptor YtvA is affected by the cellular environment and by hydration. *PLoS One* 9, e107489.
- **30.** Purcell, E.B., McDonald, C.A., Palfey, B.A., Crosson, S., (2010). An analysis of the solution structure and signaling mechanism of LovK, a sensor histidine kinase integrating light and redox signals. *Biochemistry* **49**, 6761–6770.
- Zayner, J.P., Sosnick, T.R., (2014). Factors that control the chemistry of the LOV domain photocycle. *PLoS One* 9, e87074.
- 32. Briggs, W.R., Huala, E., (1999). Blue-light photoreceptors in higher plants. *Annu Rev Cell Dev Bi.* 15, 33–62.
- 33. Christie, J.M., (2007). Phototropin blue-light receptors. Annu. Rev. Plant Biol. 58, 21–45.
- Takahashi, F., Yamagata, D., Ishikawa, M., Fukamatsu, Y., Ogura, Y., Kasahara, M., Kiyosue, T., Kikuyama, M., et al., (2007). AUREOCHROME, a photoreceptor required for photomorphogenesis in stramenopiles. PNAS 104, 19625– 19630.
- Schwerdtfeger, C., Linden, H., (2003). VIVID is a flavoprotein and serves as a fungal blue light photoreceptor for photoadaptation. *EMBO J.* 22, 4846– 4855.
- Avila-Perez, M., Hellingwerf, K.J., Kort, R., (2006). Blue light activates the sigma(B)-dependent stress response of Bacillus subtilis via YtvA. J. Bacteriol. 188, 6411–6414.
- Conrad, K.S., Manahan, C.C., Crane, B.R., (2014).
 Photochemistry of flavoprotein light sensors. *Nature Chem. Biol.* 10, 801–809.
- Herrou, J., Crosson, S., (2011). Function, structure and mechanism of bacterial photosensory LOV proteins. *Nature Rev. Microbiol.* 9, 713–723.
- Losi, A., Gärtner, W., (2008). Bacterial bilin- and flavin-binding photoreceptors. *Photochem. Photobiol. Sci.: Official J. Eur. Photochem. Assoc. Eur. Soc. Photobiol.* 7, 1168–1178.
- Glantz, S.T., Carpenter, E.J., Melkonian, M., Gardner, K. H., Boyden, E.S., Wong, G.K., Chow, B.Y., (2016).

- Functional and topological diversity of LOV domain photoreceptors. *PNAS* **113**, E1442–E1451.
- 41. Rani, R., Jentzsch, K., Lecher, J., Hartmann, R., Willbold, D., Jaeger, K.E., Krauss, U., (2013). Conservation of dark recovery kinetic parameters and structural features in the pseudomonadaceae "short" light, oxygen, voltage (LOV) protein family: implications for the design of LOV-based optogenetic tools. *Biochemistry* 52, 4460–4473.
- Krauss, U., Minh, B.Q., Losi, A., Gartner, W., Eggert, T., von Haeseler, A., Jaeger, K.E., (2009). Distribution and phylogeny of light-oxygen-voltage-blue-light-signaling proteins in the three kingdoms of life. *J. Bacteriol.* 191, 7234–7242.
- Arinkin, V., Granzin, J., Röllen, K., Krauss, U., Jaeger, K. E., Willbold, D., Batra-Safferling, R., (2017). Structure of a LOV protein in apo-state and implications for construction of LOV-based optical tools. Sci. Rep. 7, 42971.
- Endres, S., Granzin, J., Circolone, F., Stadler, A., Krauss, U., Drepper, T., Svensson, V., Knieps-Grunhagen, E., et al., (2015). Structure and function of a short LOV protein from the marine phototrophic bacterium Dinoroseobacter shibae. *BMC Microbiol.* 15, 30.
- Arinkin, V., Granzin, J., Krauss, U., Jaeger, K.E., Willbold, D., Batra-Safferling, R., (2021). Structural determinants underlying the adduct lifetime in the LOV proteins of Pseudomonas putida. FEBS J. 288, 4955–4972.
- Röllen, K., Granzin, J., Panwalkar, V., Arinkin, V., Rani, R., Hartmann, R., Krauss, U., Jaeger, K.E., et al., (2016). Signaling States of a Short Blue-Light Photoreceptor Protein PpSB1-LOV Revealed from Crystal Structures and Solution NMR Spectroscopy. J. Mol. Biol. 428, 3721– 3736.
- Zoltowski, B.D., Schwerdtfeger, C., Widom, J., Loros, J.J., Bilwes, A.M., Dunlap, J.C., Crane, B.R., (2007). Conformational switching in the fungal light sensor Vivid. Science 316, 1054–1057.
- Conrad, K.S., Bilwes, A.M., Crane, B.R., (2013). Light-induced subunit dissociation by a light-oxygen-voltage domain photoreceptor from Rhodobacter sphaeroides. *Biochemistry* 52, 378–391.
- Hendrischk, A.K., Moldt, J., Fruhwirth, S.W., Klug, G., (2009). Characterization of an unusual LOV domain protein in the alpha-proteobacterium Rhodobacter sphaeroides. *Photochem. Photobiol.* 85, 1254–1259.
- Metz, S., Jager, A., Klug, G., (2012). Role of a short light, oxygen, voltage (LOV) domain protein in blue light- and singlet oxygen-dependent gene regulation in Rhodobacter sphaeroides. *Microbiology* 158, 368–379.
- Sumi, S., Mutaguchi, N., Ebuchi, T., Tsuchida, H., Yamamoto, T., Suzuki, M., Natsuka, C., Shiratori-Takano, H., et al., (2020). Light-response of *Pseudomonas putida* KT2440 mediated by class II LitR, a photosensor homolog. *J. Bacteriol.* 202, e00146–e220.
- 52. Hemmer, S., Schulte, M., Knieps-Grunhagen, E., Granzin, J., Willbold, D., Jaeger, K.E., Batra-Safferling, R., Panwalkar, V., et al., (2023). Residue alterations within a conserved hydrophobic pocket influence light, oxygen, voltage photoreceptor dark recovery. *Photochem. Photobiol. Sci.: Official J. Eur. Photochem. Assoc. Eur. Soc. Photobiol.* 22, 713–727.
- Silby, M.W., Cerdeno-Tarraga, A.M., Vernikos, G.S., Giddens, S.R., Jackson, R.W., Preston, G.M., Zhang, X. X., Moon, C.D., et al., (2009). Genomic and genetic

- analyses of diversity and plant interactions of Pseudomonas fluorescens. *Genome Biol.* **10**, R51.
- Losi, A., Gardner, K.H., Moglich, A., (2018). Blue-Light Receptors for Optogenetics. *Chem. Rev.* 118, 10659– 10709.
- McWilliam, H., Li, W.Z., Uludag, M., Squizzato, S., Park, Y. M., Buso, N., Cowley, A.P., Lopez, R., (2013). Analysis Tool Web Services from the EMBL-EBI. *Nucleic Acids Res.* 41. W597–W600.
- Kabsch, W., Sander, C., (1983). Dictionary of protein secondary structure – pattern-recognition of hydrogenbonded and geometrical features. *Biopolymers* 22, 2577– 2637.
- Krissinel, E., Henrick, K., (2007). Inference of macromolecular assemblies from crystalline state. *J. Mol. Biol.* 372, 774–797.
- 58. Kumar, P., Bansal, M., (2012). HELANAL-Plus: a web server for analysis of helix geometry in protein structures. *J. Biomol. Struct. Dyn.* 30, 773–783.
- Halavaty, A.S., Moffat, K., (2007). N- and C-terminal flanking regions modulate light-induced signal transduction in the LOV2 domain of the blue light sensor phototropin 1 from Avena sativa. *Biochemistry* 46, 14001– 14009.
- Bocola, M., Schwaneberg, U., Jaeger, K.E., Krauss, U., (2015). Light-induced structural changes in a short light, oxygen, voltage (LOV) protein revealed by molecular dynamics simulations-implications for the understanding of LOV photoactivation. Front. Mol. Biosci. 2, 55.
- Zhao, Y., Zhang, Y., Sun, M., Zheng, Q., (2021). A theoretical study on the signal transduction process of bacterial photoreceptor PpSB1 based on the Markov state model. PCCP 23, 2398–2405.
- Diensthuber, R.P., Bommer, M., Gleichmann, T., Moglich, A., (2013). Full-length structure of a sensor histidine kinase pinpoints coaxial coiled coils as signal transducers and modulators. Structure 21, 1127–1136.
- Rinaldi, J., Fernandez, I., Shin, H., Sycz, G., Gunawardana, S., Kumarapperuma, I., Paz, J.M., Otero, L.H., et al., (2021). Dimer asymmetry and light activation mechanism in brucella blue-light sensor histidine kinase. *mBio.* 12 e00264-21.
- 64. Berntsson, O., Diensthuber, R.P., Panman, M.R., Bjorling, A., Gustavsson, E., Hoernke, M., Hughes, A.J., Henry, L., et al., (2017). Sequential conformational transitions and alpha-helical supercoiling regulate a sensor histidine kinase. *Nature Commun.* 8, 284.
- Engelhard, C., Diensthuber, R.P., Moglich, A., Bittl, R., (2017). Blue-light reception through quaternary transitions. Sci. Rep. 7, 1385.
- Berntsson, O., Diensthuber, R.P., Panman, M.R., Bjorling, A., Hughes, A.J., Henry, L., Niebling, S., Newby, G., et al., (2017). Time-resolved X-ray solution scattering reveals the structural photoactivation of a light-oxygen-voltage photoreceptor. *Structure* 25, 933–938.e3.
- 67. Zayner, J.P., Mathes, T., Sosnick, T.R., Kennis, J.T.M., (2019). Helical contributions mediate light-activated conformational change in the LOV2 domain of avena sativa phototropin 1. ACS Omega 4, 1238–1243.
- Kawano, F., Aono, Y., Suzuki, H., Sato, M., (2013).
 Fluorescence imaging-based high-throughput screening of fast- and slow-cycling LOV proteins. PLoS One 8, e82693.

- Pettersen, E.F., Goddard, T.D., Huang, C.C., Couch, G.S., Greenblatt, D.M., Meng, E.C., Ferrin, T.E., (2004). UCSF Chimera—a visualization system for exploratory research and analysis. *J. Comput. Chem.* 25, 1605–1612.
- Wang, C., Sang, J., Wang, J., Su, M., Downey, J.S., Wu, Q., Wang, S., Cai, Y., et al., (2013). Mechanistic insights revealed by the crystal structure of a histidine kinase with signal transducer and sensor domains. *PLoS Biol.* 11, e1001493.
- Mechaly, A.E., Sassoon, N., Betton, J.M., Alzari, P.M., (2014). Segmental helical motions and dynamical asymmetry modulate histidine kinase autophosphorylation. *PLoS Biol.* 12, e1001776.
- Mechaly, A.E., Soto Diaz, S., Sassoon, N., Buschiazzo, A., Betton, J.M., Alzari, P.M., (2017). Structural coupling between autokinase and phosphotransferase reactions in a bacterial histidine kinase. Structure 25 (939–944), e3.
- Marina, A., Waldburger, C.D., Hendrickson, W.A., (2005). Structure of the entire cytoplasmic portion of a sensor histidine-kinase protein. *EMBO J.* 24, 4247–4259.
- 74. Bick, M.J., Lamour, V., Rajashankar, K.R., Gordiyenko, Y., Robinson, C.V., Darst, S.A., (2009). How to switch off a histidine kinase: crystal structure of Geobacillus stearothermophilus KinB with the inhibitor Sda. *J. Mol. Biol.* 386, 163–177.
- Cai, Y., Su, M., Ahmad, A., Hu, X., Sang, J., Kong, L., Chen, X., Wang, C., Shuai, J., Han, A., (2017). Conformational dynamics of the essential sensor histidine kinase Walk. Acta Crystallogr D Struct Biol. 73, 793–803.
- Studier, F.W., (2005). Protein production by auto-induction in high-density shaking cultures. *Protein Expr. Purif.* 41, 207–234.
- 77. von Stetten, D., Giraud, T., Carpentier, P., Sever, F., Terrien, M., Dobias, F., Juers, D.H., Flot, D., et al., (2015). In crystallo optical spectroscopy (icOS) as a complementary tool on the macromolecular crystallography beamlines of the ESRF. *Acta Crystallogr. D Biol. Crystallogr.* 71, 15–26.
- Flot, D., Mairs, T., Giraud, T., Guijarro, M., Lesourd, M., Rey, V., van Brussel, D., Morawe, C., et al., (2010). The ID23-2 structural biology microfocus beamline at the ESRF. J. Synchrotron Radiat. 17, 107–118.
- de Sanctis, D., Beteva, A., Caserotto, H., Dobias, F., Gabadinho, J., Giraud, T., Gobbo, A., Guijarro, M., et al., (2012). ID29: a high-intensity highly automated ESRF beamline for macromolecular crystallography experiments exploiting anomalous scattering. *J. Synchrotron Radiat.* 19, 455–461.
- Bourenkov, G.P., Popov, A.N., (2010). Optimization of data collection taking radiation damage into account. *Acta Crystallogr. D Biol. Crystallogr.* 66, 409–419.
- 81. Kabsch, W., (2010). Xds, *Acta crystallographica Section D. Biological crystallography*. 66, 125–132.
- Winn, M.D., Ballard, C.C., Cowtan, K.D., Dodson, E.J., Emsley, P., Evans, P.R., Keegan, R.M., Krissinel, E.B., et al., (2011). Overview of the CCP4 suite and current developments. *Acta Crystallogr. D Biol. Crystallogr.* 67, 235–242.
- Adams, P.D., Afonine, P.V., Bunkoczi, G., Chen, V.B., Davis, I.W., Echols, N., Headd, J.J., Hung, L.W., et al., (2010). PHENIX: a comprehensive Python-based system for macromolecular structure solution. *Acta Crystallogr. D Biol. Crystallogr.* 66, 213–221.

- 84. Emsley, P., Cowtan, K., (2004). Coot: model-building tools for molecular graphics. *Acta Crystallogr. D Biol. Crystallogr.* **60**, 2126–2132.
- Abraham, M.J., Murtola, T., Schulz, R., Páll, S., Smith, J. C., Hess, B., Lindahl, E., (2015). GROMACS: High performance molecular simulations through multi-level parallelism from laptops to supercomputers. *SoftwareX* 1–2, 19–25.
- **86.** Lindorff-Larsen, K., Piana, S., Palmo, K., Maragakis, P., Klepeis, J.L., Dror, R.O., Shaw, D.E., (2010). Improved side-chain torsion potentials for the Amber ff99SB protein force field. *Proteins* **78**, 1950–1958.
- Essmann, U., Perera, L., Berkowitz, M.L., Darden, T., Lee, H., Pedersen, L.G., (1995). A smooth particle mesh ewald method. J. Chem. Phys. 103, 8577–8593.
- Kraulis, P.J., (1991). Molscript a program to produce both detailed and schematic plots of protein structures. *J. Appl. Cryst.* 24, 946–950.
- 89. Merritt, E.A., Bacon, D.J., (1997). Raster3D: photorealistic molecular graphics. *Methods Enzymol.* 277, 505–524.
- 90. Williams, T. & Kelley, C. (1986) Gnuplot 5.0: an interactive plotting program.